NOAA Technical Memorandum ERL ETL-268

# WIND, WAVE, STRESS, AND SURFACE ROUGHNESS RELATIONSHIPS FROM TURBULENCE MEASUREMENTS MADE ON R/P *FLIP* IN THE SCOPE EXPERIMENT

**A REPORT FOR THE DOD ASAP PROGRAM**
**ENVIRONMENTAL SENSING PROGRAM ELEMENT (P.ETL.2909)**

C.W. Fairall
A.A. Grachev
A.J. Bedard
R.T. Nishiyama

Environmental Technology Laboratory
Boulder, Colorado
April 1996

**UNITED STATES DEPARTMENT OF COMMERCE**

**Michael Kantor**
**Secretary**

NATIONAL OCEANIC AND ATMOSPHERIC ADMINISTRATION

D. JAMES BAKER
Under Secretary for Oceans and Atmosphere/Administrator

Environmental Research Laboratories

James L. Rasmussen
Director

NOTICE

Mention of a commercial company or product does not constitute an endorsement by NOAA/ERL. Use for publicity or advertising purposes, of information from this publication or concerning proprietary products or the tests of such products, is not authorized.

For sale by the National Technical Information Service, 5285 Port Royal Road, Springfield, VA 22061

## CONTENTS

ABSTRACT ..... 1

1. BASIC INFORMATION ..... 1

2. BACKGROUND ..... 3

3. THE VELOCITY PROFILE IN CONVECTIVE CONDITIONS ..... 5

4. ROUGHNESS RELATIONSHIPS IN PURE AND LOCAL FREE CONVECTION ..... 7
   - 4.1 Local Free Convection ..... 8
   - 4.2 Pure Free Convection ..... 9
   - 4.3 Summary ..... 14

5. SCOPE DATA ANALYSIS ..... 15
   - 5.1 Background on the SCOPE Measurements ..... 15
   - 5.2 Mean Charnock Constant Analysis ..... 18
   - 5.3 Variability Analysis ..... 18
   - 5.4 Surface Wave Aspects ..... 23
   - 5.5 Discussion ..... 26

6. CONCLUSIONS ..... 31

7. ACKNOWLEDGMENTS ..... 32

8. REFERENCES ..... 32

# Wind, Wave, Stress, and Surface Roughness Relationships from Turbulence Measurements Made on R/P *FLIP* in the SCOPE Experiment

## A Report for the DoD ASAP Program Environmental Sensing Program Element (P.ETL.2090)

C. W. Fairall, A. A. Grachev,[1] A. J. Bedard, and R. T. Nishiyama

**ABSTRACT.** This report describes an investigation of the behavior of the sea surface roughness length, $z_0$, and the Charnock coefficient, $\alpha$, and their relation to the surface fluxes for moderate and light winds. The Charnock constant is an index of the gravity wave contribution to the surface roughness. The study focuses on parameterization of $z_0$ in the convective limit when conventional approaches of determination of $z_0$ cannot be applied. In this "smooth flow" regime, gravity waves do not contribute to $z_0$. In pure free convective conditions, the convective profile behavior extends down to the molecular sublayer, so no log-profile region exists. The conventional approach also does not take into account large-scale coherent structures embracing the entire convective boundary layer (CBL) These circulations create random gusts in the surface layer (the "gustiness effect") that tend to enhance the fluxes and affect the surface roughness. Such parameterizations (e.g., the Charnock relation) are used in all numerical models of fluxes and radar scattering from the ocean.

The new approach has been applied to measurements made on the Scripps Institute Floating Instrument Platform (R/P *FLIP*) in the San Clemente Ocean Probing Experiment (SCOPE) in September 1993. These measurements include data of covariance and inertial-dissipation turbulent fluxes, bulk variables, height of the CBL, and direct-wave measurements in the wind-speed range from 0.3 to 11 m $s^{-1}$. A "preaveraging" analysis indicates a mean Charnock constant for the SCOPE data of 0.0125 [compared to 0.011 obtained from the Tropical Ocean-Global Atmosphere (TOGA) Coupled Ocean-Atmosphere Response Experiment (COARE) data]. Examining the wind-speed dependence of individual observations, it is found that $\alpha$ tends to increase as mean wind velocity goes below 4 m $s^{-1}$. However, the sea surface does not become aerodynamically rough again at light winds as previously suggested by Wu (1994). Using simple wave information (significant wave height and period of the dominant waves), we have also looked at wave-parameter dependences of the Charnock constant. Comparisons with data from the North Sea lead us to conclude that wave age alone is not sufficient to describe variability in the Charnock parameter. Rather, much of the increase of $\alpha$ at low wind speeds is associated with wind directions that are different from that of the dominant wave direction (300°).

## 1. BASIC INFORMATION

Estimation of the momentum flux above the sea surface and its dependence on the aerodynamic roughness length, $z_0$, is a classic problem of air-sea interaction. This problem plays a key role in climate research, remote sensing, and numerical modeling of atmospheric and oceanic processes. The standard method is the so-called bulk flux algorithm, where the fluxes are parameterized in terms of the bulk meteorological variables (wind speed, water temperature,

[1]On leave from the Institute of Atmospheric Physics, 3 Pyzhevsky, Moscow 109017, Russia.

air temperature, and humidity) and empirical transfer coefficients. In neutral conditions (i.e., air and water at the same temperature), these transfer coefficients are mathematically related to the roughness lengths. When air and water are at different temperatures, stability corrections must be applied. The mathematical structure for the bulk flux algorithm is well established (e.g., Fairall et al., 1995a); the empirical coefficients are based on decades of direct measurements of the fluxes and the associated bulk variables (see reviews by Geernaert, 1990; Kraus and Businger, 1994).

The relevance of the wind-wave-stress problem to ocean remote sensing, and radar scattering from the ocean surface in particular, is quite complex. Clearly, the surface waves (swell, wind waves, and capillary waves) are caused by wind stress. Generally, the stress is the result of an interaction of the wind and the surface. The drag of the sea surface is usually partitioned into "form drag" associated with the larger gravity waves and "viscous drag" associated with interactions with the interface (either smooth or with capillary waves). Radars typically Bragg scatter from waves on the order of the radar wavelength (centimeters for normal x-band systems). The wind stress on the ocean surface increases roughly with the square of the mean wind speed as does the significant wave height (see Pierson, 1990). However, at a given wind speed, the stress can be highly variable; much of the variability is believed to be associated with variations in the two-dimensional wave spectrum. In recent years, theoretical models have appeared which purport to allow calculation of the surface stress spectrum from a specification of the wave spectrum (e.g., Makin et al., 1995). Which part of the wave spectrum causes the wind stress is still controversial. Makin et al. (1995) claimed that stress is dominated by waves on the order of 1-m wavelength and that capillary waves do not contribute, while Bourassa et al. (1995) claimed that capillary waves dominate stress for wind speeds below 2 m $s^{-1}$. Thus, it is obvious that variations in wind stress associated with variations in wind speed and stability cause variations in the surface waves responsible for the backscatter return of centimeter-wave radars. It is not known if these radar-sensitive waves have any direct influence on the stress or its parametric coefficient, $z_0$.

Sorting out the competing influences of atmospheric variability (wind gusts, boundary-layer scale coherent structures, and mesoscale processes) and oceanic variability (internal waves, oceanic coherent structures, and surface currents) on the local wave spectrum (and the resultant radar returns) requires considerable advancement in knowledge of these processes. In this report, we will examine one aspect of the problem: the average relationship between the mean meteorological structure (wind speed, sea-air temperature difference, etc.) and meteorological characterization of the surface roughness. Our emphasis will be on the low wind-speed regime where present theories have conceptual inadequacies and where surface manifestations of oceanic dynamical processes (thermal or wave spectral features) are most likely to be observable.

Our approach in this report is to outline the traditional theory and describe its failures. Then, we generalize the theory to correctly handle convective effects. We clarify several misconceptions that have caused confusion in the past. This leads to a natural distinction between what we term "pure" free convection and "local" free convection. Simple analytical

expressions are developed that allow computation of $z_0$ from measured meteorological variables (wind speed and the air-sea fluxes). We then use data from the San Clemente Ocean Probing Experiment (SCOPE) to test our new theory. SCOPE was conducted near San Clemente Island, California, aboard the Scripps Institute Floating Instrument Platform (R/P *FLIP*) in September 1993. We are also able to examine the present standard parametric representation of $z_0$ as the sum of gravity wave form drag (Charnock relation) and aerodynamically smooth (viscous) contributions. The hypothesized dependence of Charnock's constant on surface wave spectral parameters is also investigated.

## 2. BACKGROUND

Estimation of the roughness length, $z_0$, in the atmospheric surface layer is based on the presumed existence of a logarithmic velocity profile

$$u(z) = \frac{u_*}{\kappa} \ln(z/z_0) \ , \tag{1}$$

where $u_*$ is the friction velocity and $\kappa \approx 0.4$ is the von Kármán constant. The friction velocity is a representation of the stress (sideways force per unit area) exerted by the wind on the ocean surface:

$$u_* = \left[-\overline{wu}\right]^{1/2} \ , \tag{2}$$

where the term in the bracket in (2) represents the usual covariance of turbulent fluctuations of the vertical and streamwise velocities. The actual turbulent surface stress is obtained by multiplying $\overline{wu}$ by the density of air. Thus, (1) and (2) represent the relationship between the mean wind speed and the wind force on the ocean.

The aerodynamic roughness length, $z_0$, is related to the physical roughness of the surface. For the ocean, there are a number of parameterizations for the aerodynamic roughness length in terms of sea state. The Charnock (1955) relation

$$z_0 = \alpha u_*^2/g \tag{3}$$

follows from dimensional reasoning and is the generally recognized way of relating aerodynamic roughness length to the surface gravity wave spectrum (hence, the use of $g$). The Charnock "constant" $\alpha$ in (3) is between 0.01 and 0.035, and in the general case it is hypothesized to depend on some properties of the surface wave spectrum. The mostly commonly suggested property to characterize this dependence is the wave age, $C_p/u_*$,

$$\alpha = f(C_p/u_*) \ , \tag{4}$$

where $f(C_p/u_*)$ is some presently unknown function of the wave age, and $C_p$ is the phase velocity for waves corresponding to the frequency peak of wave spectrum.

As the wind speed decreases (calm weather conditions), the sea surface becomes aerodynamically smooth and $z_0$ is proportional to the viscous sublayer thickness (see e.g., Monin and Yaglom, 1971):

$$z_0 = 0.11\,\nu/u_* \,, \tag{5}$$

where $\nu$ is the kinematic viscosity of air. The usual physical interpretation of smooth flow is that the actual surface roughness elements (ripples for the ocean) are smaller than the molecular sublayer thickness. The transition from one regime to another is described by the roughness Reynolds number

$$Re_r = u_* z_0/\nu \,. \tag{6}$$

When $Re_r < 0.13$, the flow is said to be aerodynamically smooth and this value usually corresponds to winds over the sea surface less than about 2–3 m s$^{-1}$. For $Re_r > 2.0$, the flow can be described as aerodynamically rough. Over the sea surface, rough flow occurs for wind speed greater than about 7–8 m s$^{-1}$ (Geernaert, 1990; Volkov et al., 1992; Fairall et al., 1995a). Combining (3) and (5), we obtain an equation which applies to both regimes (Smith, 1988):

$$z_0 = \alpha u_*^2/g + 0.11\,\nu/u_* \,. \tag{7}$$

There is some evidence that relationship (7) breaks down under strongly convective conditions where, according to Monin-Obukhov similarity, the mean wind speed and, therefore, the friction velocity, tend to zero. In fact, according to Wu (1994) the sea surface becomes aerodynamically rough again under light winds. We will return to this controversy later. Note that we can alternatively express (7) in terms of the roughness Reynolds number

$$Re_r = 0.11 + \frac{\alpha u_*^3}{g\nu} \,. \tag{8}$$

Over the past four decades, significant advances have been made in understanding atmospheric turbulence in the convective boundary layer (CBL). In strong convection with no (or very weak) mean wind, the traditional concept of local flux-gradient correspondence underlying Monin-Obukhov similarity theory breaks down. Recently, it has been concluded that in such conditions, semiorganized coherent structures develop embracing the entire CBL and these convective circulations can create random perturbation gusts in the surface layer. It has been recognized that such large-scale convective flow patterns produce local logarithmic height distributions for velocity and temperature profiles in the layer attached to the large-scale eddies (Kraichnan, 1962). This generates local horizontal velocity shear ("minimum friction velocity") which crucially affects the heat/mass transfer (Businger, 1973).

Some progress has been made recently in theoretically analyzing the effects of large-scale convection on turbulent transfer in the CBL (Schumann, 1988; Sykes et al., 1993; Stull, 1994; Zilitinkevich, 1994). The gustiness concept has been applied to bulk methods of calculating air-sea fluxes that cover all wind speeds including the case of strong convection. In this approach, the vector mean wind speed $u$ is replaced by an effective speed $S$ that is the vector sum of $u$ and $u_g = 1.25\, w_*$ (the "gustiness assumption") of Fairall et al. (1995a):

$$S^2 = G^2 u^2 = \left[1 + (1.25 w_*/u)^2\right] u^2 \,, \tag{9}$$

where $G$ is the gustiness parameter and

$$w_* = \left[(g z_i/\rho)\,(H_s/Tc_p + 0.61\, H_l/l)\right]^{1/3} = (F_B\, z_i)^{1/3} \tag{10}$$

is the Deardorff (1970) convective velocity scale. The quantity $F_B$ is the surface buoyancy flux ($g$ is the acceleration of gravity, $\rho$ is air density, $H_s$ is the sensible heat flux, $H_l$ is the latent heat flux, $T$ is air temperature, $c_p$ is the specific heat of air at constant pressure, and $l$ is the latent heat of evaporation). The gustiness effect was originally introduced to enhance scalar flux estimates in light winds. However, even when including gustiness, the conventional approach may still lead to a singularity in extremely light winds. This singularity is associated with application of the log-law where no log-regime exists (Godfrey and Beljaars, 1991).

Thus, it seems reasonable that the next step must be extension of the approach developed by Schumann (1988), Sykes et al. (1993), Stull (1994), Zilitinkevich (1994), and Fairall et al. (1995a) to the aerodynamic roughness length of the sea surface under strongly convective conditions. The goal of this aspect of our work is to develop an alternative approach capable of including the effects of the CBL scale structures on sea surface roughness length, $z_0$, under strongly convective conditions. To do this, we must reexamine the basic matching assumptions of the molecular subrange and the turbulent surface layer. For these purposes, data obtained under convective conditions from R/P *FLIP* in SCOPE in September 1993 are used.

## 3. THE VELOCITY PROFILE IN CONVECTIVE CONDITIONS

Historically, to include the dependence on atmospheric stability for the velocity profile, (1) can be rewritten (Panofsky, 1963; Paulson, 1970) in the form

$$u(z) = (u_*/\kappa)\left[\ln(z/z_0) - \Psi_u(z/L) + \Psi_u(z_0/L)\right] \,, \tag{11}$$

where $u(z_0) = 0$ by definition and the function $\Psi_u$ obeys

$$\Psi_u(\xi) = \int_0^{\xi} \frac{\left[1 - \phi_u(x)\right]}{x}\, dx \ . \tag{12}$$

Here, $\xi = z/L$ and $\phi_u = (\kappa z/u_*)(du/dz)$ is the dimensionless gradient function. The term $\Psi_u(z_0/L)$ is negligible for $|z_0/L| \ll 1$ and it is usually omitted in (11). Also,

$$L = -u_*^3/(\kappa F_B) \tag{13}$$

is the Obukhov length scale.

For unstable conditions, the "Kansas-type" function (Businger et al., 1971)

$$\phi_u(\xi) = (1 - 16\xi)^{-1/4} \tag{14}$$

is commonly used to describe the velocity gradient profile. Carrying out integration of (12) with $\phi_u$ defined by (14) have

$$\Psi_u = \Psi_{\text{Kansas}} = 2\ln\left[(1+x)/2\right] + \ln\left[(1+x^2)/2\right] - \tan^{-1}(x) + \pi/2 \ , \tag{15}$$

where $x = (1 - 16\xi)^{1/4}$. It should be noted that (15) does not have the theoretically correct free convection limit where both velocity and temperature profiles vary asymptotically as $z^{-1/3}$. It has been previously demonstrated that using (15) at low wind speeds leads to results that are not physically reasonable (see Godfrey and Beljaars, 1991; Delage and Girard, 1992; Sugita et al., 1995).

There are several ways to avoid this problem. One of them is replacement of the -1/4 exponent in (14) by -1/3:

$$\phi_u = (1 - a\xi)^{-1/3} \ , \tag{16}$$

where the numerical coefficient $a = 12$ (Delage and Girard, 1992, p. 27) or $a = 12.87$ (Fairall et al., 1995a). According to experimental data by Kader and Yaglom (1990), $\phi_u/\kappa = 1.7\,(\xi/\kappa)^{-1/3}$ in the convective regime that corresponds to $a = 1.7^{-3}\kappa^{-4} \approx 8$. Carrying out the integration of (12) with $\phi_u$ given by (16), we obtain (Fairall et al., 1995a)

$$\Psi_u = \Psi_{\text{convective}} = 1.5\ln\left[(y^2 + y + 1)/3\right] - \sqrt{3}\tan^{-1}\left[(2y+1)/\sqrt{3}\ \right] + \pi/\sqrt{3} \ , \tag{17}$$

where $y = (1 - a\xi)^{1/3}$. Another asymptotically correct form of $\phi_u$ is the KEYPS equation [see, e.g., Panofsky (1963); Monin and Yaglom (1971)]. Note that Paulson (1970) integrated the KEYPS equation and obtained a relationship for function $\Psi_u$. Fairall et al. (1995a) proposed interpolating between the Kansas equation (15) and free convection (17):

$$\Psi_u = \left[\Psi_{\text{Kansas}} + \xi^2 \Psi_{\text{convective}}\right] / (1 + \xi^2) \ . \tag{18}$$

Equation (18) gives good agreement with standard Kansas-type profile expressions for near-neutral stratification and obeys the -1/3 asymptotic convective limit dependence on stability.

Let us illustrate the key role of the term $\Psi_u(z_0/L)$ in (8), as well as using the key role of the function having correct asymptotic behavior in the free convective limit. Expanding (17) for $|-a\xi| \geq 1$, we obtain

$$\Psi_u = \ln(-\xi) + \ln(a/3^{3/2}) - \sqrt{3}\,\pi/6 + 3(-a\xi)^{-1/3} + \text{higher order} \ . \tag{19}$$

For pure free convection (i.e., where $-L$ is so small that $-z_0/L$ is large: $|z/L| \geq |z_0/L| \geq 1/a$), we find

$$\Psi_u(z/L) - \Psi_u(z_0/L) = \ln(z/z_0) + 3\left[(-az/L)^{-1/3} - (-az_0/L)^{-1/3}\right] . \tag{20}$$

Substituting (20) into (11), the $\ln(z/z_0)$ term vanishes and we have the correct expression for the velocity profile in the strict convective limit. On the other hand, if we use a relationship for the function $\phi_u$ that does not obey the -1/3 law, and/or we neglect the $\Psi_u(z_0/L)$ term, the logarithmic term does not disappear in the final expression. While (20) is mathematically correct for the conditions stated above, it can be misleading and has been erroneously applied in the past. Clearly, since $z_0$ is 5 orders of magnitude smaller than typical observation heights, the first one-third power term can be neglected, and we can solve for $z_0$ in terms of measured wind speed and friction velocity. This interpretation is usually in error for three reasons: (1) even in the lightest winds, the requirement that $-z_0/L$ is significant is rarely met over the open ocean; (2) it does not account for gustiness; and (3) in conditions where the basic requirement is met, we must reexamine the entire basis of matching turbulent and molecular sublayer profiles.

## 4. ROUGHNESS RELATIONSHIPS IN PURE AND LOCAL FREE CONVECTION

Our objective is to sort out the conceptual problems discussed in Sec. 3 and, if possible, obtain simple analytical formulas for determination of $z_0$ under convective conditions (light winds). It is important to note that, for most of the experimental data presented here, the typical situation is characterized by the presence of a logarithmic sublayer between the molecular and convective sublayers. In other words, the pure convective state does not exist. Thus, our

reference point of measurements (11 m) is in the convective ($z^{-1/3}$) sublayer, but $z_0$ is not and (20) cannot be applied. In this circumstance, we can use (19) from the measurement height down to the lower limit of its applicability at a height, $z_{tr}$, where the profile begins to make the transition to logarithmic behavior. From near the surface up, we use (1) to describe the log-profile. Matching of these two profiles provides a relation between $z_0$ and the measured variables.

### 4.1 Local Free Convection

The first step in this solution is to examine the convective part of the velocity gradient profile [$(-az/L) \geq 1$] where we have from (16)

$$\phi_u = (-az/L)^{-1/3} - \frac{1}{3}(-az/L)^{-4/3} + \frac{2}{9}(-az/L)^{-7/3} - \frac{14}{81}(-az/L)^{-10/3} + \ldots . \qquad (21)$$

Integrating this equation from the transition height $z_{tr} = -L/a$ to the reference height $z_r = 11$ m, we find that

$$(\kappa/u_*)\left[u(z_r) - u(z_{tr})\right] = 2.82 - 3(-az_r/L)^{-1/3} + 0.25(-az_r/L)^{-4/3} + \ldots . \qquad (22)$$

In fact, the numerical coefficient 2.82 is a consequence of the expansion and the further substitution of the value $z_{tr} = -L/a$ in the series: $2.82 \approx 3 - 0.25 + (2/21) - (14/270) + (5/165)$. Note that the leading term $(-az/L)^{-1/3}$ in the expansion of $\phi_u$ gives the well-known velocity gradient profile in the convective regime (Monin and Yaglom, 1971; Kader and Yaglom, 1990):

$$\frac{du}{dz} = A_u u_*^2 F_B^{-1/3} z^{-4/3} . \qquad (23)$$

Here, $A_u = 1.7$ according to the field data by Kader and Yaglom (1990) and $A_u = (a\kappa^4)^{-1/3} \approx 1.5$ for our calculations ($a = 12.87$ and $\kappa = 0.4$).

For the near-surface part of the profile, we expand (16) for $(-az/L) \leq 1$ and we obtain

$$\phi_u = 1 - \frac{1}{3}(-az/L) + \frac{2}{9}(-az/L)^2 - \frac{14}{81}(-az/L)^3 + \ldots . \qquad (24)$$

Integrating (24) from $z = z_0$ to $z_{tr} = -L/a$,

$$(\kappa/u_*)\, u(z_{tr}) = -\ln(-az_0/L) - 0.27 + \frac{1}{3}(-az_0/L) - \frac{1}{9}(-az_0/L)^2 + \frac{14}{243}(-az_0/L)^3 + \ldots . \qquad (25)$$

Combining (22) and (25) to eliminate $u(z_{tr})$ and keeping only the most significant terms gives

$$z_0 = (-L/a)\exp\left\langle[\kappa u(z_r)/u_*] + 2.55 - 3(-az_r/L)^{-1/3}\right\rangle . \quad (26)$$

Using this condition and taking into account the "gustiness assumption" (9), (26) becomes

$$z_0 = (-L/a)\exp\left\langle-[\kappa G u(z_r)/u_*] + 2.55 - 3(-az_r/L)^{-1/3}\right\rangle . \quad (27)$$

Thus, (27) is a simple closed relationship for determination of sea surface roughness length under local free convective conditions. Note that (1) is invalid in this case because it ignores buoyancy effects and, while (11) with (17) is valid, it is a transcendental equation that must be solved iteratively. In this equation, $L$ is determined from (13), $w_*$ described by (10), the coefficient $a = 12.87$ (Fairall et al., 1995a), and $u(z_r)$ is the measured mean wind vector magnitude at the reference height $z_r$.

### 4.2 Pure Free Convection

To investigate the pure free convection case (where the $z^{-1/3}$ dependence extends to the viscous sublayer), we must next examine the necessary conditions for matching the profiles at the interface between the turbulent sublayer where the velocity profile is given by (11) and the viscous interfacial sublayer directly adjacent to the solid or the water surface. Here, we follow the procedure of Liu et al. (1979; hereafter, LKB). First, we assume that the velocity profile in this viscous sublayer is described by

$$u(z)/u_* = C_u\left[1 - \exp\left(-zu_*/C_u\nu\right)\right] , \quad (28)$$

where the parameter $C_u$ describes the total normalized velocity change across the viscous sublayer. LKB required (28) to match the turbulent profile as described by (1) both in magnitude and in slope at certain matching height $z_v$. For a given value of $Re_r$, LKB solved (1) and (28) for $C_u$ and $z_v$. For smooth flow ($Re_r = 0.11$), this matching occurs for $z_v = 47\ \nu/u_*$ and $C_u = 16$. This procedure worked until $Re_r = 0.8$ (where $z_v = 17\ \nu/u_*$ and $C_u = 9$). For $Re_r > 0.8$, no solution exists, and LKB resorted to other means that are not relevant to the present discussion of light winds.

We will duplicate the LKB approach with several modifications: we use (7) to specify $z_0$, we include gustiness, and we use (11) with (18) to describe the turbulent profile. A solution is found iteratively for a given specification of wind vector magnitude, sea-air temperature difference ($\Delta T$), and the inversion height consistent with the conditions stated above. Figures 1a–c show examples of matching the velocity profiles for different stability conditions. The solid lines represent the viscous profile (28), and the dashed line corresponds to (11). Dotted vertical lines on these graphs correspond to the matching height $z_v$ (M point), $z_{tr}$ (C point), and the reference height $z_r = 11$ m (Z point). The point of intersection of the dashed line with the

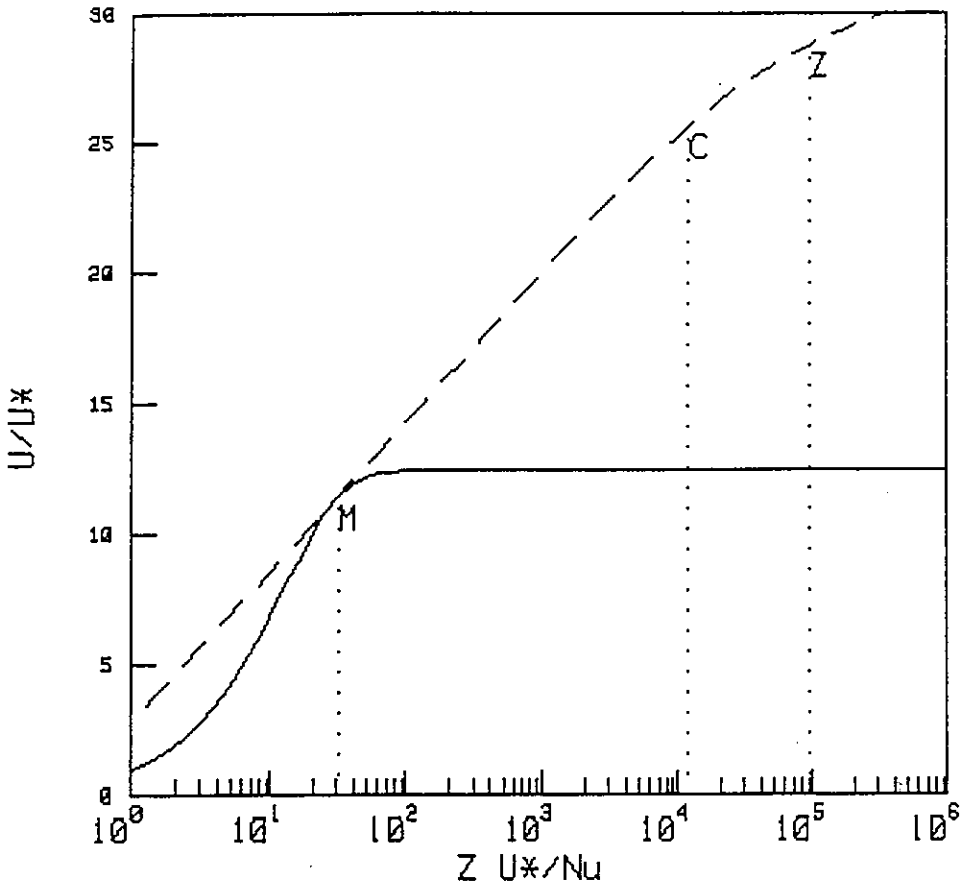


FIGURE 1a. Matching of the velocity profiles for the turbulent layer [Eq. (11), dashed line] and the viscous sublayer [Eq. (28), solid line] based on the LKB model. M indicates the matching point; C, the transition to the convective part of the profile; and Z, the height of the measurement for $u(z_r) = 4$ m s$^{-1}$, $\Delta T = 2.5$ K, $Re = 0.35$, and $C_u = 12.2$.

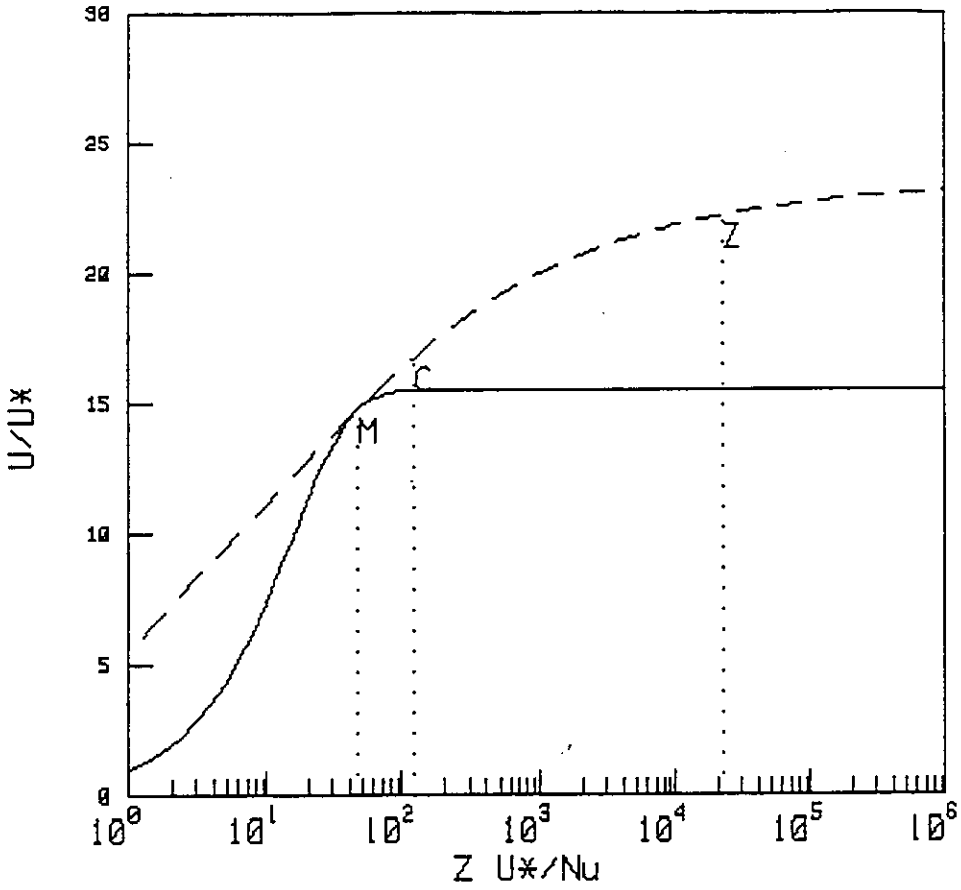


FIGURE 1b. Matching of the velocity profiles for the turbulent layer [Eq. (11), dashed line] and the viscous sublayer [Eq. (28), solid line] based on the LKB model. M indicates the matching point; C, the transition to the convective part of the profile; and Z, the height of the measurement for $u(z_r) = 0.5$ m s$^{-1}$, $\Delta T = 2.5$ K, $Re = 0.113$, and $C_u = 15.5$.

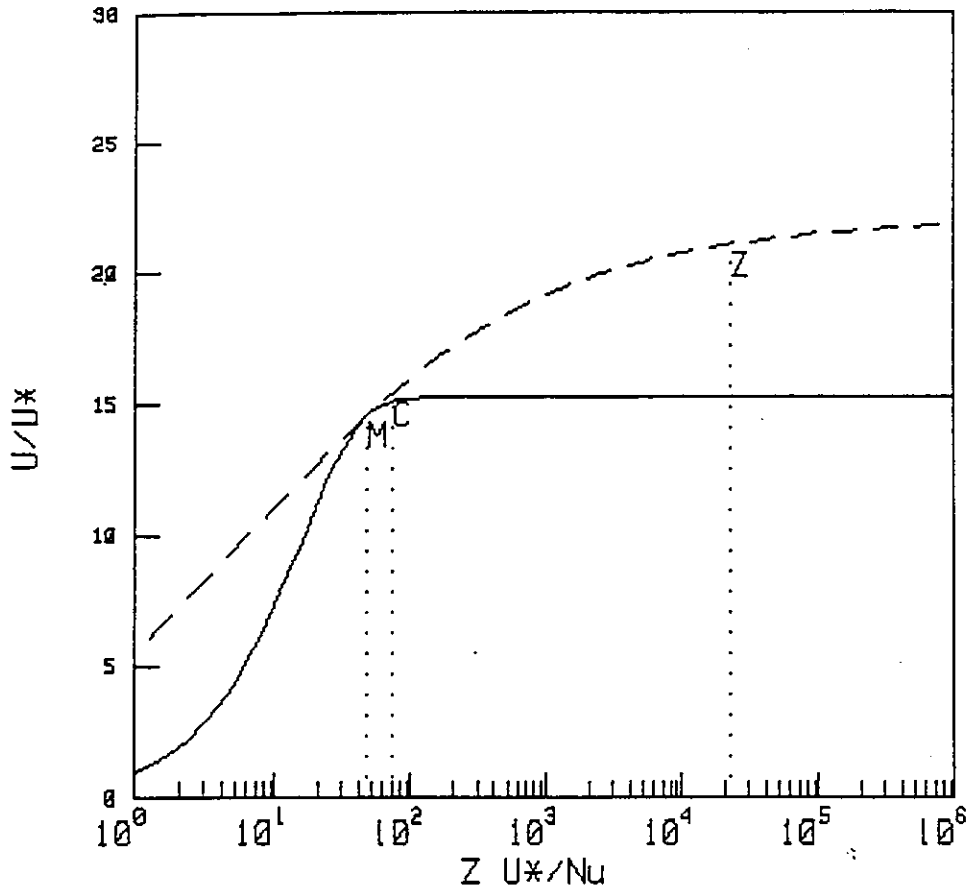


FIGURE 1c. Matching of the velocity profiles for the turbulent layer [Eq. (11), dashed line] and the viscous sublayer [Eq. (28), solid line] based on the LKB model. M indicates the matching point; C, the transition to the convective part of the profile; and Z, the height of the measurement for $u(z_r) = 0.25$ m s$^{-1}$, $\Delta T = 4$ K, $Re = 0.113$, and $C_u = 15.3$.

horizontal axis is determined by the roughness length $z_0$. The linear part of the dashed line corresponds to log-profile. Unstable stratification is increased from Fig. 1a [$u(z_r) = 4$ m s$^{-1}$, a typical SCOPE wind speed] through Fig. 1b [$u(z_r) = 0.5$ m s$^{-1}$, one of the lighter SCOPE wind speeds] to Fig. 1c [$u(z_r) = 0.25$ m s$^{-1}$]. Other parametric details are given in the figure captions. It is interesting to note that, with increasing instability, more of the velocity change takes place in the viscous interfacial sublayer rather than in the turbulent region (compare Figs. 1a and 1c). Even though Fig. 1c represents the extreme in convective conditions one might expect to encounter in the SCOPE region, the convectively induced curvature in the turbulent profile has only a modest effect on the matching parameters, and smooth flow values from LKB could be used.

The requirement of profile matching enables one to evaluate $z_0$ and other quantities ($u_*$, $T_* = H_s/c_p \rho u_*$, $L$) when the external parameters [$u(z_r)$ and $\Delta T$] are specified. Thus, explicit but complex numerical calculations give the following values for the situation presented in Fig. 1a: $u_* = 0.15$ m s$^{-1}$, $-L = 10.6$ m, and $z_0 = 3.5\ 10^{-5}$ m; in Fig. 1b: $u_* = 0.034$ m s$^{-1}$, $-L = 0.69$ m, and $z_0 = 5\ 10^{-5}$ m; and in Fig. 1c: $u_* = 0.034$ m s$^{-1}$, $-L = 0.41$ m, and $z_0 = 5\ 10^{-5}$ m. Comparison of these exact values of $z_0$ with those obtained from (27) shows good agreement.

We expect (27) to be valid if point C lies between points M and Z, which is clearly the case in Figs. 1a,b. This upper requirement can be stated more precisely as the reference height $z_r$ should be inside the convective sublayer, i.e., $z_r \geq z_{tr}$:

$$-\xi = -z_r/L \geq 1/a \approx 0.08 \ . \tag{29}$$

Note that most of the SCOPE measurements meet the condition (29). The lower boundary can be evaluated from the condition that $z_{tr} \geq z_\nu$. Obviously, the flow can be assumed smooth for the case of light winds (see Fig. 1c), so $z_\nu \approx 47\ \nu/u_*$ as discussed above. Using this relationship and $z_{tr} = -L/a$, we obtain

$$-L/a \geq 47\ \nu/u_* \ . \tag{30}$$

When (30) is just violated, the convective profile behavior extends down to the molecular sublayer, so no log-profile region exists in the actual profile because the viscous sublayer form (28) follows from that point on the profile. Substituting $L$ from (13) and using values of $H_s \approx 10$ W m$^{-2}$ and $H_l \approx 40$ W m$^{-2}$ for the typical SCOPE conditions, we estimate a minimum threshold of $u_* = 0.03$ m s$^{-1}$ for (27) to remain valid. Values of the friction velocity for SCOPE are rarely less than about 0.04 m s$^{-1}$, and in one case only does $u_* = 0.035$ m s$^{-1}$.

Note that the inequality (30) can be rewritten as

$$-R_i = \nu F_B / u_*^4 \leq (47\ \kappa a)^{-1} = 0.00413 \ . \tag{31}$$

Here, $R_i$ is the so-called viscous sublayer Richardson number (Grachev, 1990). The parameter $R_{i*}$ describes the transition to the pure free convective regime where the log-profile does not exist. In this case ($-R_i \geq 0.00413$), (27) is not valid. Assuming that the matching conditions do not significantly modify $C_u$ and $z_v$, then $z_0$ can be evaluated from (20):

$$z_0 = \left[ z_r^{-1/3} + \frac{\kappa u G (a \kappa F_B)^{1/3}}{3 u_*^2} \right]^{-3} \approx \left[ \frac{3 u_*^2}{u G} \right]^3 (\kappa^4 a F_B)^{-1} . \tag{32}$$

Here, $z_0$ is defined as in the case of log-profile, i.e., a height for which $u = 0$. While (32) is certainly of theoretical interest, its applicability is rare over the ocean because random gusts usually produce sufficient local friction velocity to exceed 0.03 m s$^{-1}$.

### 4.3 Summary

We wish to summarize the conclusions of this section. Also, the expansion of (19) allows us to replace the arithmetic constant 2.55 in (27) with the factor $\ln(3^{3/2}) + \pi\sqrt{3}/6$. Here, we give the formulas for $z_0$ for the three possible regimes.

For $(-z_0/L) < (-z_r/L) < 1/a$:

$$z_0 = z_r \exp(-\kappa u G / u_*) . \tag{33}$$

For $(-z_0/L) < 1/a < (-z_r/L)$:

$$z_0 = (-\sqrt{27}\, L/a) \exp\left[ -\kappa u G/u_* + \pi\sqrt{3}/6 - 3 (-a z_r/L)^{-1/3} \right] . \tag{34}$$

For $1/a < (-z_0/L) < (-z_r/L)$:

$$z_0 = \frac{27}{a \kappa F_B} \left[ \frac{u_*^2}{\kappa u G} \right]^3 . \tag{35}$$

## 5. SCOPE DATA ANALYSIS

### 5.1 Background on the SCOPE Measurements

We have applied (27) to turbulence measurements made on R/P *FLIP* in SCOPE held off southern California in September 1993. This complex experiment was performed by the NOAA Environmental Technology Laboratory to investigate air-sea interactions with remote and *in situ* measurements. R/P *FLIP* was moored about 15 km northwest of the NW point of San Clemente Island with good open ocean exposure for northwest winds (Kropfli and Clifford, 1994). The measurements included bulk meteorological variables, covariance fluxes of sensible heat, latent heat, and stress, radiative fluxes, turbulent spectra, and sea surface temperature. Details of the measurement system can be found in Fairall et al. (1995b). Inversion height was obtained from radiosonde temperature and humidity profiles using sondes launched from the R/V *Titan* and the U.S. Navy installation on nearby San Nicolas Island. Surface wave parameters were measured by an Air Sea Interaction Array (ASIA) designed and constructed for SCOPE. This system included underwater pressure sensors to measure gravity waves, as well as a capacitance wire capillary wave array that responded to frequencies higher than 25 Hz. These sensors were mounted on a mast deployed from one of the horizontal booms on R/P *FLIP*. The underwater pressure sensors located about 1.7 m underwater were in a square array, on aluminum, guyed struts 2.1 m long. The atmospheric pressure sensors were located directly above the underwater pressure sensors, 2 m above the mean ocean surface. The capillary wave array consisted in four capacitance wires in a square array, 1 cm on a side. This array was mounted between the arms of a "U"-shaped length of aluminum channel equipped with a buoy so that it would "wave ride." The wave-riding arm was oriented in the direction from which most wave activity was expected without being downstream of R/P *FLIP* (i.e., the northwest).

The entire SCOPE time series for several key variables is shown in Fig. 2. The marine surface layer was, with the exception of a few days of fog, unstable for the duration of SCOPE; winds were not strong, averaging around 4 m $s^{-1}$, and a northwest swell was moderate but almost always present. The maximum value of wind velocity was about 11 m $s^{-1}$ on one brief occasion. During several runs, the environmental conditions were characterized by mostly unstable stratification when wind velocities were below 1 m $s^{-1}$. Wind directions were predominantly from the northwest, but influence of the mesoscale land-sea contrast caused some modulation on a diurnal cycle (apparent as oscillations in the wind and friction velocity trace in Fig. 2). Several episodes of weakening and turning winds occurred in which the wind direction and sea direction were out of balance. These episodes caused loss of streamwise $\overline{wu}$ and tended to cause nonzero crosswind ($\overline{wv}$). In Fig. 2, the wind speed and friction velocity appear to have a very high correlation. This is examined more closely in Fig. 3, where we see that $u/u_*$ is in fact highly variable. Only a small part of this variability can be explained by the stability effects accounted for in (11). This additional variability leads to apparent variations in $z_0$, of which only a small fraction can be explained by (7).

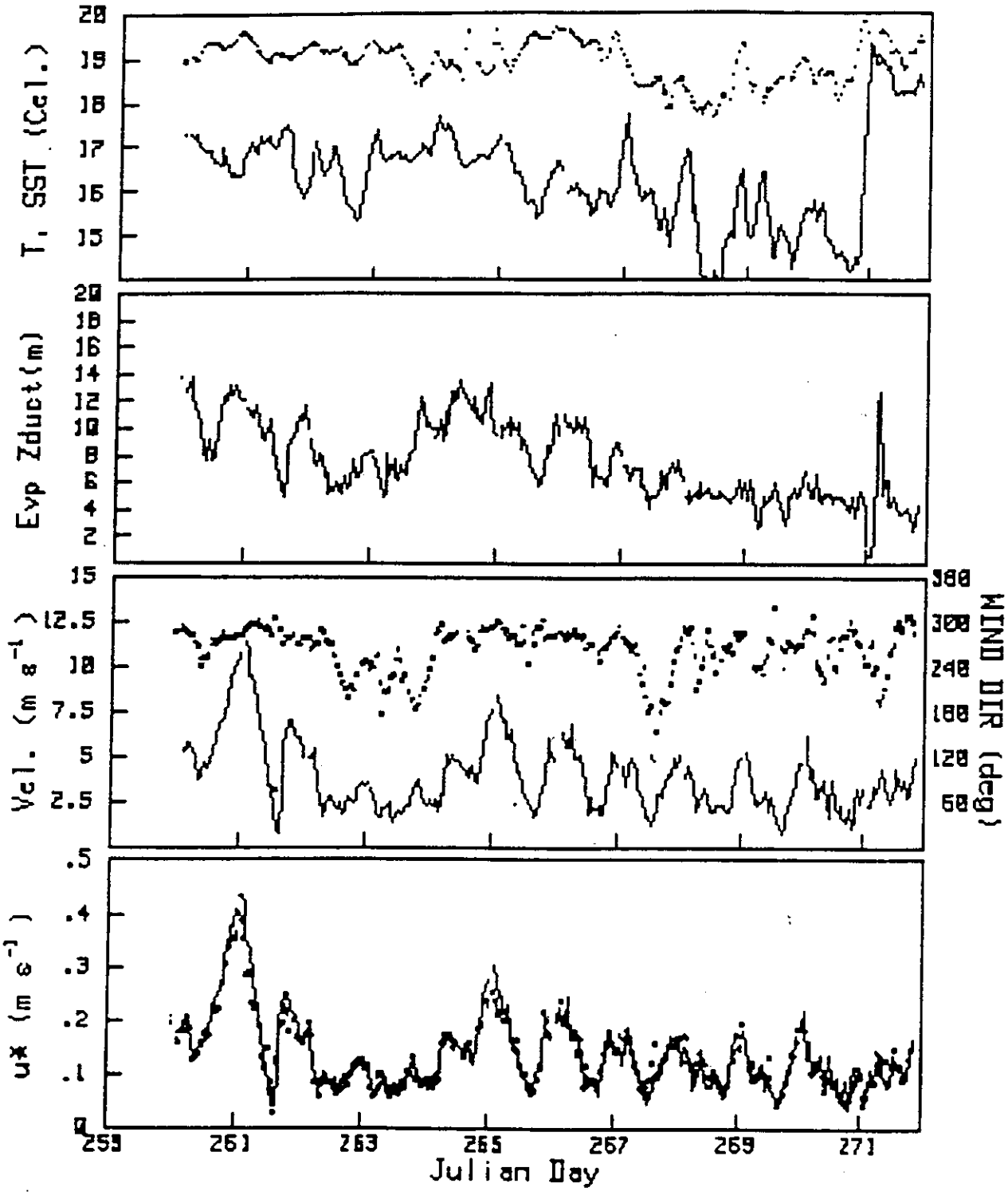


FIGURE 2. Atmospheric surface-layer observations made from R/P *FLIP* for 12 days during SCOPE: friction velocity $u_*$ (lower panel), mean wind velocity $u$ (line) and direction (dots), evaporation duct height, air temperature (line), and sea surface temperature (dots, upper panel). Julian day 261 corresponds to September 18, 1993.

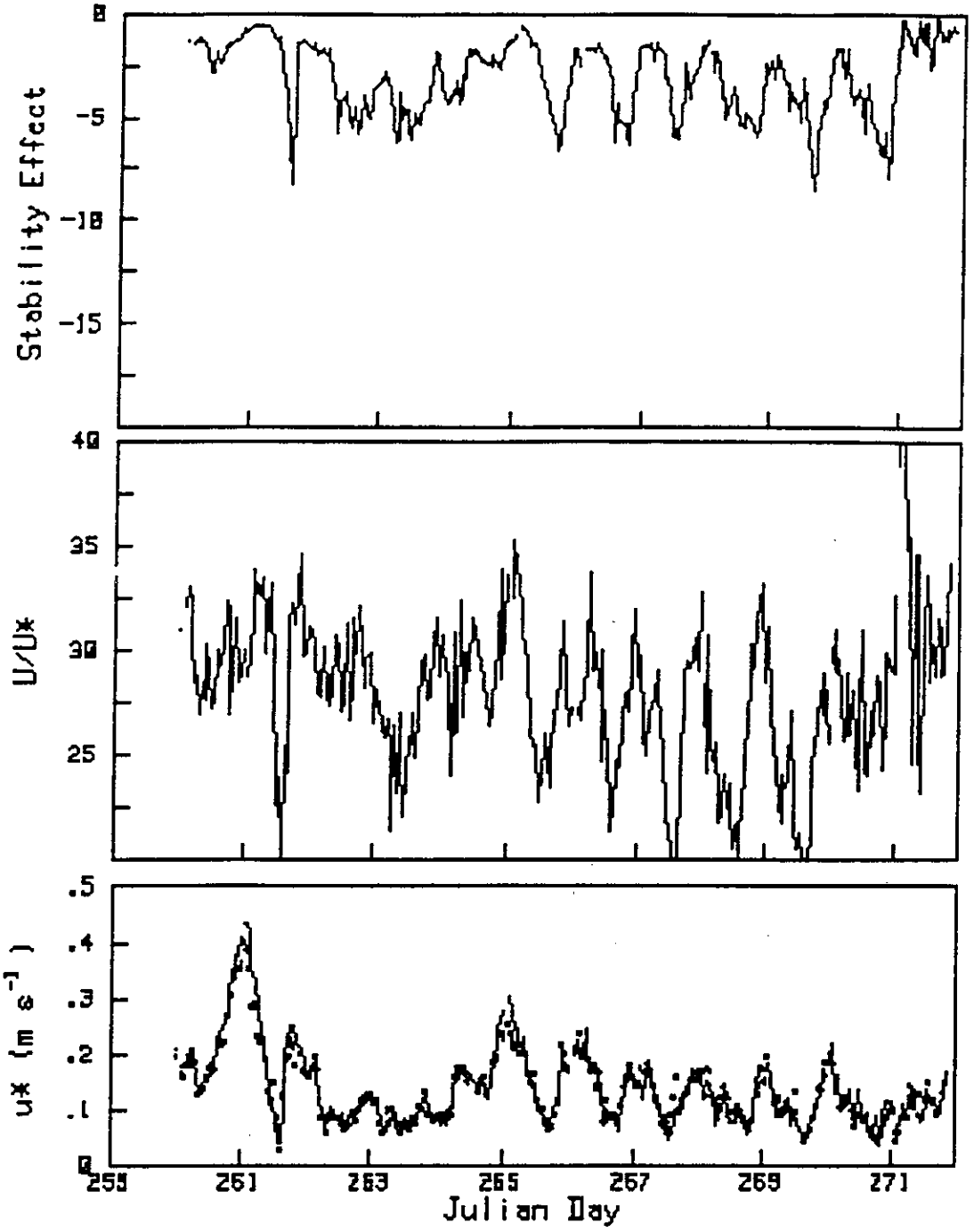


FIGURE 3. Time series of friction velocity $u_*$ (lower panel), the ratio $u/u_*$, and the Monin-Obukhov stability profile correction $\Psi_u(\xi)$ using (11) and (17). Julian day 261 correspond to September 18, 1993.

### 5.2 Mean Charnock Constant Analysis

The first step in our analysis is to compute a mean value for $\alpha$ that represents the overall dataset. We have already performed such an analysis on the Tropical Ocean-Global Atmosphere (TOGA) Coupled Ocean-Atmosphere Response Experiment (COARE) dataset obtained in three cruise legs on the R/V *Moana Wave* in the tropical western Pacific in 1992–1993. The experiment and analysis have been described by Fairall et al. (1995a). Using direct measurements of $u_*$ and $z_0$, we compute $\alpha$ from (7). This process works poorly as $u_*$ becomes small because we are taking the difference of two large numbers subject to measurement errors. Fairall et al. (1995a) attempted to reduce the scatter in this analysis by averaging the fluxes and mean quantities in wind-speed categories of approximately 1 m $s^{-1}$ bin width. Their results for the COARE data are shown in Fig. 4, where $\alpha$ is shown as a function of $Re_r$. Using inertial-dissipation values for $u_*$, they obtained a mean value of $\alpha = 0.011$ for COARE. We have followed the same procedure, except we have used covariance values for $u_*$ for wind speed above 4 m $s^{-1}$. We would have preferred to use covariance values for the entire range, but we felt they might be compromised by tidal currents (which were not measured) at low wind speeds. The results of this analysis are shown in Fig. 5; a mean value of $\alpha = 0.0125$ was obtained.

### 5.3 Variability Analysis

The analysis of Sec. 5.2 suggests that the mean Charnock constant from the tropical western Pacific is, on average, applicable to the SCOPE data. (The difference between a value of 0.011 and 0.0125 is a few percent in stress.) Because we are also interested in short-term variability, we have analyzed individual 50-min averages. The results for roughness length are given in Fig. 6 and roughness Reynolds number in Fig. 7. The scatter for $z_0$ is typically one order of magnitude, but it is much larger at low wind speeds and decreases as wind speed increases. For 10 m $s^{-1}$ wind speeds, the scatter is quite small. This is partly a result of the wind-speed dependence of the sampling error (Fairall et al., 1990). The time-average properties we compute from our measurements are only estimates of the true ensemble average properties fluxes we need. The uncertainty of any measurement is proportional to the standard deviation that characterizes the variability of the quantity in question divided by the square root of the number of independent samples taken in the averaging period. For fixed sensors, the number of independent samples varies inversely with the wind speed. For example, we can estimate the sampling uncertainty for covariance stress values by

$$\delta(\overline{wu}) = \sigma_u \sigma_w \left[\frac{2z}{u\mathrm{T}}\right]^{1/2}, \tag{36}$$

where T is the total duration of the sample in seconds. For wind speeds of 1 m $s^{-1}$, the mean $\overline{wu}$ is 0.002 (m $s^{-1}$)$^2$, and the uncertainty is 0.009; for 4 m $s^{-1}$, the corresponding values are 0.018 and 0.007; for 8 m $s^{-1}$, they are 0.050 and 0.005. Thus, it is clear why hourly values of covariance-derived $u_*$ values are difficult to apply to roughness length analyses for light winds.

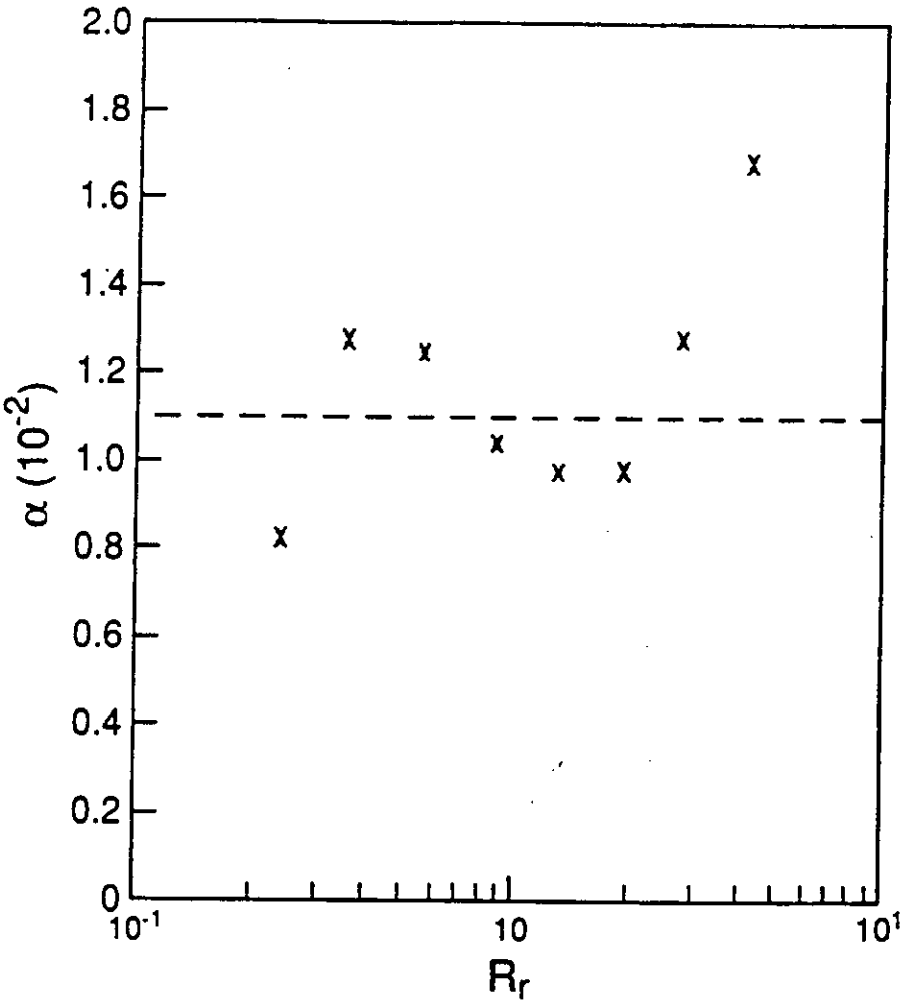


FIGURE 4. Charnock constant, $\alpha$, versus bulk-derived roughness Reynolds number, $Re_r$, for the COARE data (Fairall et al., 1995a). The dashed line corresponds to a mean value of $\alpha = 0.011$.

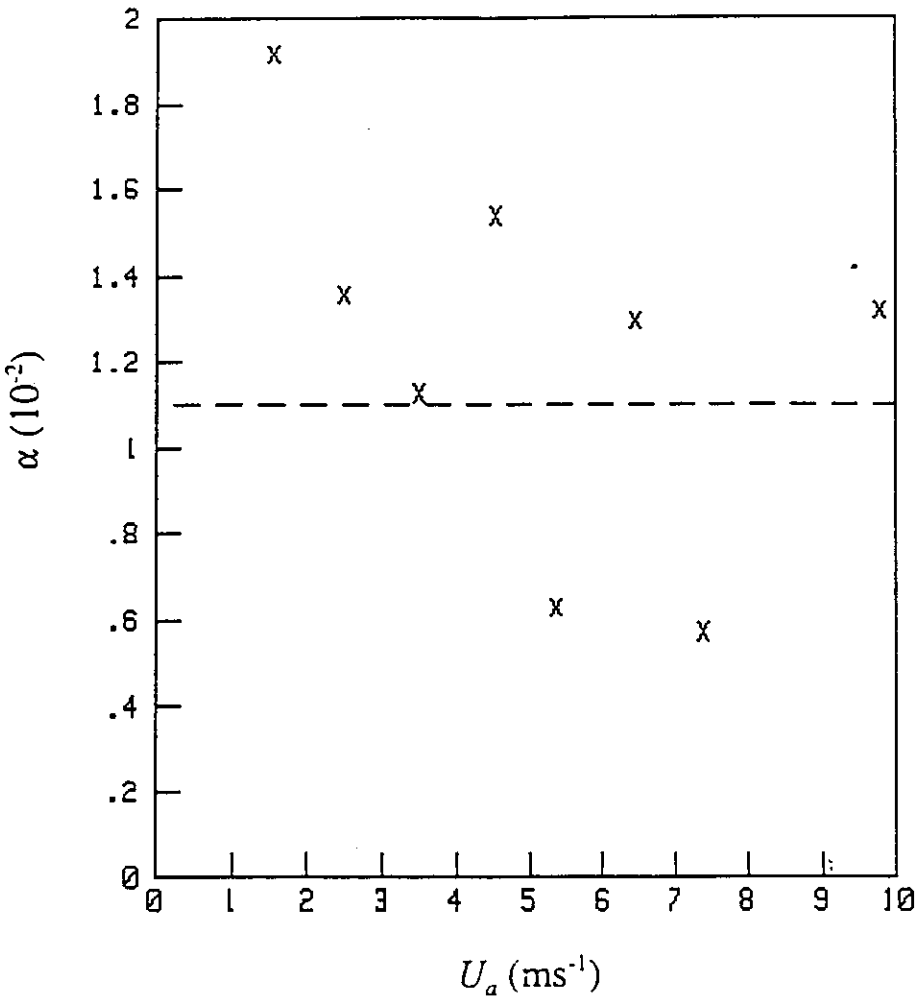


FIGURE 5. Charnock constant, $\alpha$, versus mean wind speed for SCOPE data (mean value, $\alpha = 0.0125$).

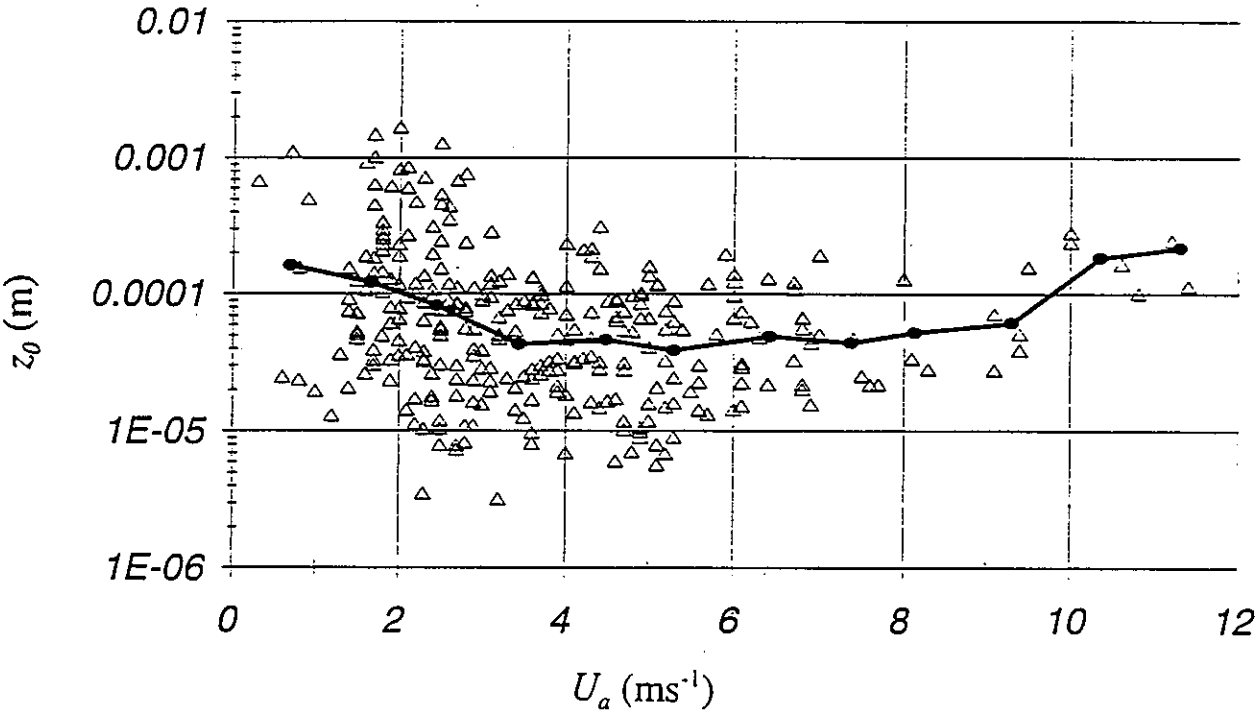


FIGURE 6. Individual data points (50-min averages) of the sea surface roughness length, $z_0$, as a function of the 11-m wind speed for SCOPE data. The values of $z_0$ are estimated from (27) for $\xi \leq -0.08$ and from (3) for $\xi \geq -0.08$. The solid line links mean value points that have been averaged in wind-speed bins with 1 m s$^{-1}$ width.

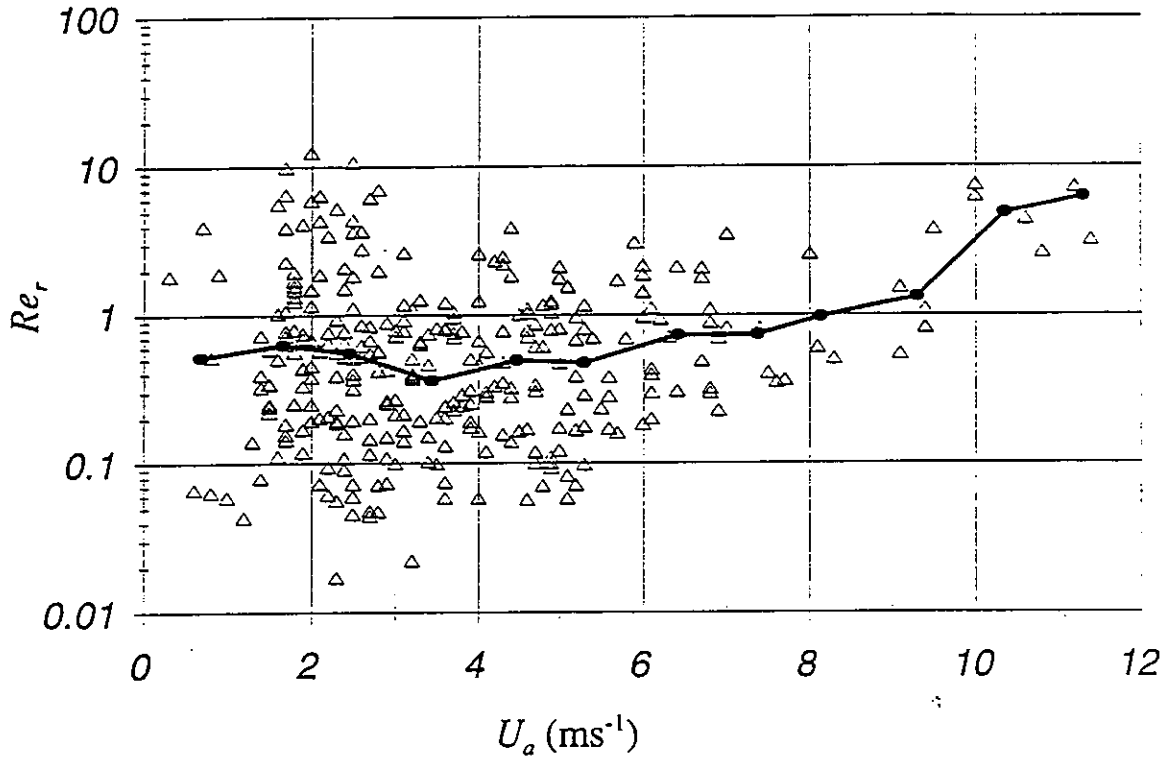


FIGURE 7. Individual data points (50-min averages) of the roughness Reynolds number, $Re_r$, as a function of the 11-m wind speed for SCOPE data. The solid line links mean value points that have been averaged in wind-speed bins with 1 m s$^{-1}$ width.

Inertial-dissipation values are subject to much less sampling uncertainty, but are not true direct measurements and require an empirical function to obtain $u_*$. Sampling variability also affects mean meteorological variables (wind speed, etc.), but the intrinsic variability compared to the mean value is much greater for fluxes than for simple first moments.

Notice in Fig. 7 that the values of $Re_r$ do not approach the expected values of 0.11 [see Eq. (8)] in the low wind-speed limit. This means that $\alpha$ (Fig. 8) does not remain constant but begins to increase in the low wind-speed regime. This increase is less apparent in Fig. 5, partly because of the nonlinearity of the extraction of $\alpha$ from the preaveraged data. In the next section, we explore the possibility that this discrepancy can be explained by the surface wave field. However, $Re_r$ clearly does not approach a value of 2.0 in the low wind-speed limit. Thus, the sea surface does not become aerodynamically rough as predicted earlier by Wu (1994). We believe that this contradictory result by Wu was the result of using (33) instead of (34).

### 5.4 Surface Wave Aspects

The literature is rich with speculations and measurements of the influence of wave parameters on stress and/or the Charnock constant. Toba and Koga (1986) suggested that $\alpha$ is proportional to wave age (but they clearly restrict this to the local wind-wave component and state that swell must be ignored); the JONSWAP group suggested $\alpha$ goes as the -1/2 power of wave age (Geernaert, 1990); and empirical measurements by Smith et al. (1992) showed a very clear -1 power with wave age. Huang et al. (1986) presented a theoretical model with a positive power law for small wave age and a negative power law for large wave age. They also gave a method to include the effects of wave height on roughness. Hsu (1974) suggested that $\alpha$ was proportional to wave slope.

Root-mean-squared wave height and the frequency of the spectral peak are available at present from the ASIA measurements for this analysis. These are the simplest characterizations of an often complex two-dimensional spectrum. In the near future, we expect information on the direction of the principal waves. The time series of wave data is shown in Fig. 9. Note that peaks in rms wave height (here expressed as the significant wave height, $H_{1/3} = 4 * \text{rms}$) roughly correspond to the peaks in $u_*$. However, the correlation is not perfect and often the wave amplitude peaks lag the $u_*$ peaks by several hours. This is a normal property of waves developing after an increase in the winds and stress. Also, notice that there are numerous decreases in $u_*$ that are not associated with a decrease in waves. These decreases are believed to be local wind decreases caused by mesoscale land-sea interactions on a diurnal cycle and occur because the experiment was conducted on the edge of the Los Angeles basin. Farther out to sea, there is little or no diurnal variation of the winds, and the waves generated in that area propagate into our observation region. This also explains the unexpected anticorrelation of wave phase speed and $u_*$. The swells propagating into the region have long periods (large phase speeds) that are not associated with local light winds. Only the strong wind events of September 18 and 24 represent situations where the local winds and waves are well coupled. This lack of wave decay

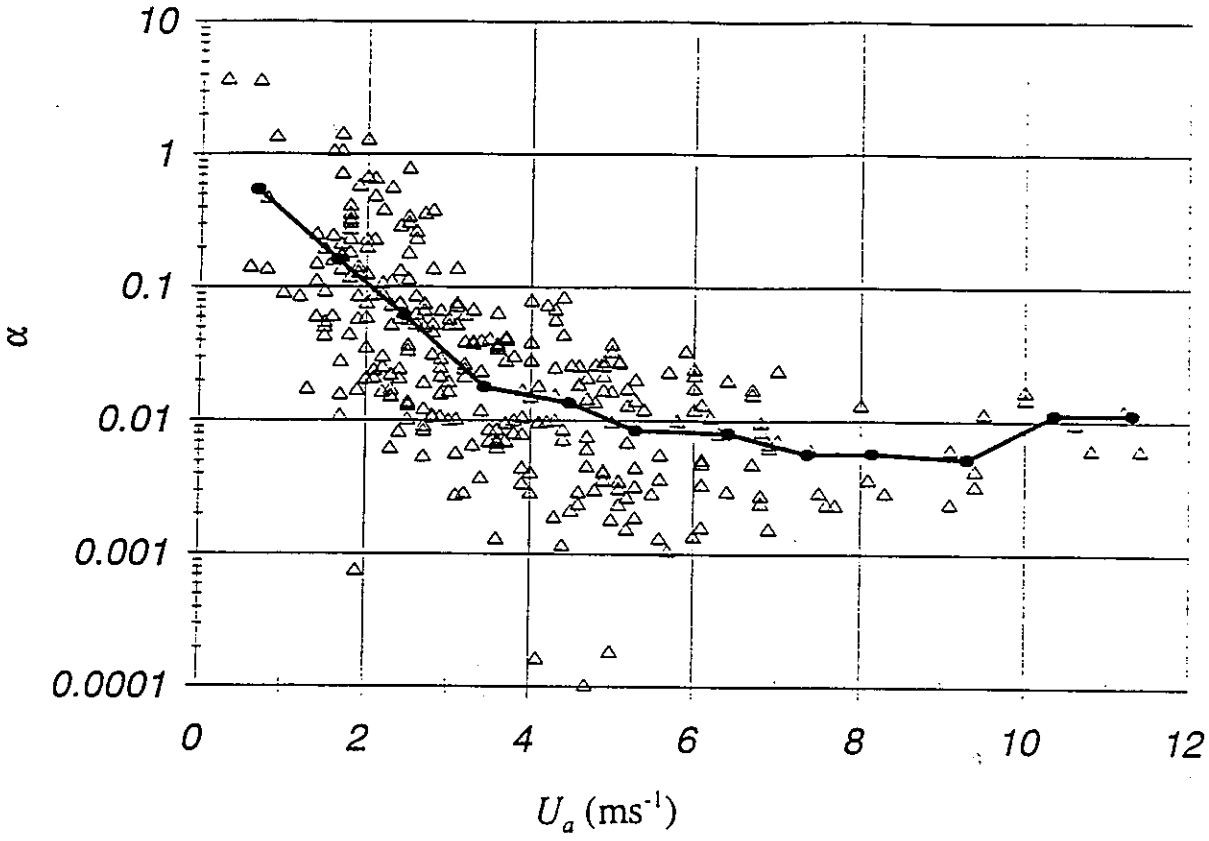


FIGURE 8. Individual data points (50-min averages) of the Charnock constant, $\alpha$, as a function of the 11-m wind speed for SCOPE data. The solid line links mean value points that have been averaged in wind-speed bins with 1 m s$^{-1}$ width.

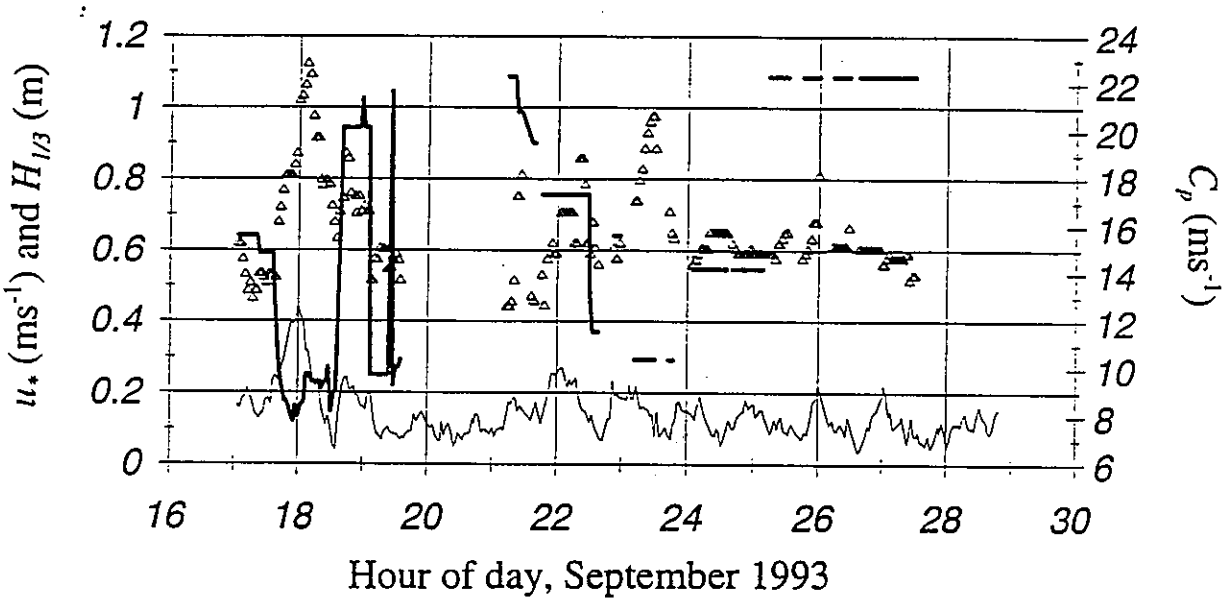


FIGURE 9. The time series of the friction velocity, $u_*$ (thin line), wave phase speed, $C_p$ (heavy line), and significant wave height, $H_{1/3}$ (triangles), obtained during SCOPE.

in light winds is emphasized in Fig. 10, where significant wave height is plotted as a function of mean wind speed. Several empirical curves giving the average equilibrium wave height as a function of wind speed are also shown. Viewed this way, the lack of correlation between wind speed and wave height is striking. There are also wind direction changes associated with this mesoscale modulation of the wind field. However, the direction of the waves was much more constant. The importance of this is illustrated by a plot of $\alpha$ versus wind direction (Fig. 11). Note the cluster of points around the dominant wind direction (300°) with a value of $\alpha$ close to 0.01; for wind directions west of 300°, $\alpha$ tends to be much larger.

A scatter plot of $\alpha$ versus wave age is shown in Fig. 12 along with the fit to the data of Smith et al. (1992). Clearly, the Smith data fall outside the range of most of our observations, but the parametric dependence on wave age is consistent with ours where they overlap. It is also obvious that the majority of our data exhibit very large wave ages, indicative of the domination by swell. Of course, it must be noted that their data were obtained in shallow water with wind speeds in the 10–15 m $s^{-1}$ range, while ours are from deep water with winds in the 1–8 m $s^{-1}$ range. Smith et al. (1992) cautioned against "self correlation" that is produced by plotting one quantity against another when both contain a common variable ($u_*$ in our case) that is subject to error, a possibility that cannot be ruled out here. Also, note that for wind directions near 300°, an asymptotic value of 0.01 appears reasonable. Similarly, in Fig. 13 we show the normalized roughness versus inverse wave-age plot suggested by Huang et al. (1986). Curves for their m parameter equal to 5 and 7 are indicated in the figure. Their theory clearly does not fit this data.

### 5.5 Discussion

The evidence presented here suggests that the standard model of $z_0$ as expressed by (7) does not, even when gustiness and convection are included, explain all of the observed features of the SCOPE data. A simple parameterization of $\alpha$ in terms of wave age would remove very little unexplained variability. The implication is that we have not obtained a universal solution. We can, however, offer a physical hypothesis to explain the SCOPE observations.

- We begin with three observations about waves: the wave heights, direction, and phase speeds are only weakly correlated with the local wind speed, and our observations are strongly influenced by waves propagating in from elsewhere. Thus, an equilibrium wind-wave balance does not exist, particularly for the light wind cases.
- Second, we note that the mean stress vector is observed to begin to deviate significantly from the mean wind direction at about 4 m $s^{-1}$, and this deviation increases until at the lowest wind speeds the mean streamwise covariance is zero, but the cross-stream covariance is larger than expected from the bulk model.
- Third, we note that $\alpha$ is unusually large for light winds and that the stress is relatively large for these conditions even though they represent the largest wave ages.

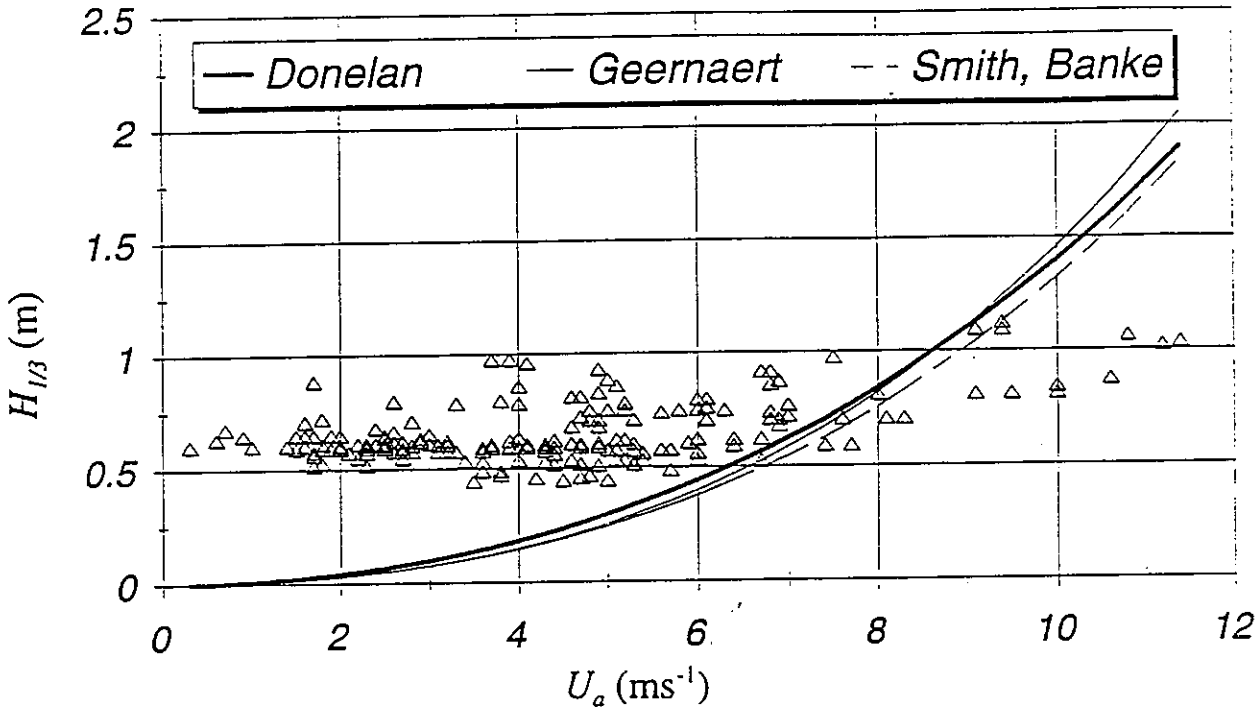


FIGURE 10. Significant wave height $H_{1/3}$ versus the mean wind speed at 11 m. The lines are empirical dependences taken from Pierson (1990).

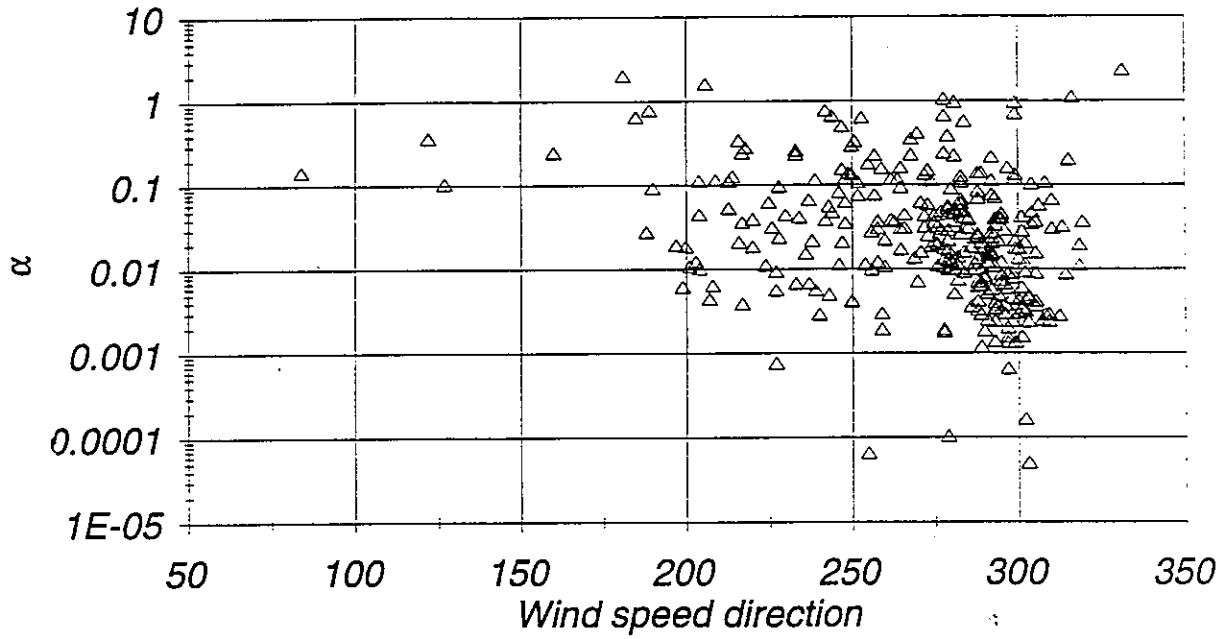


FIGURE 11. Charnock coefficient as a function of wind direction.

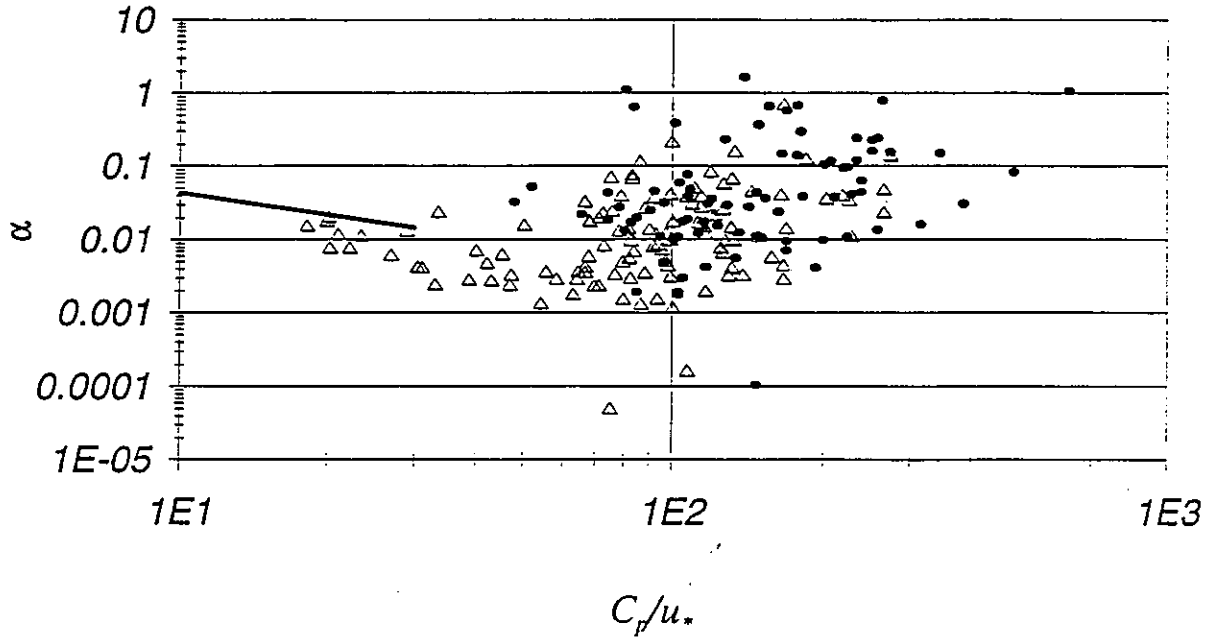


FIGURE 12. Dependence of $\alpha$ on wave age, $C_p/u_*$. The solid line is a regression of the form $\alpha = 0.48\ (C_p/u_*)^1$ from Smith et al. (1992). The open triangles are for wind directions within 20° of 300°; the solid circles are for other wind directions.

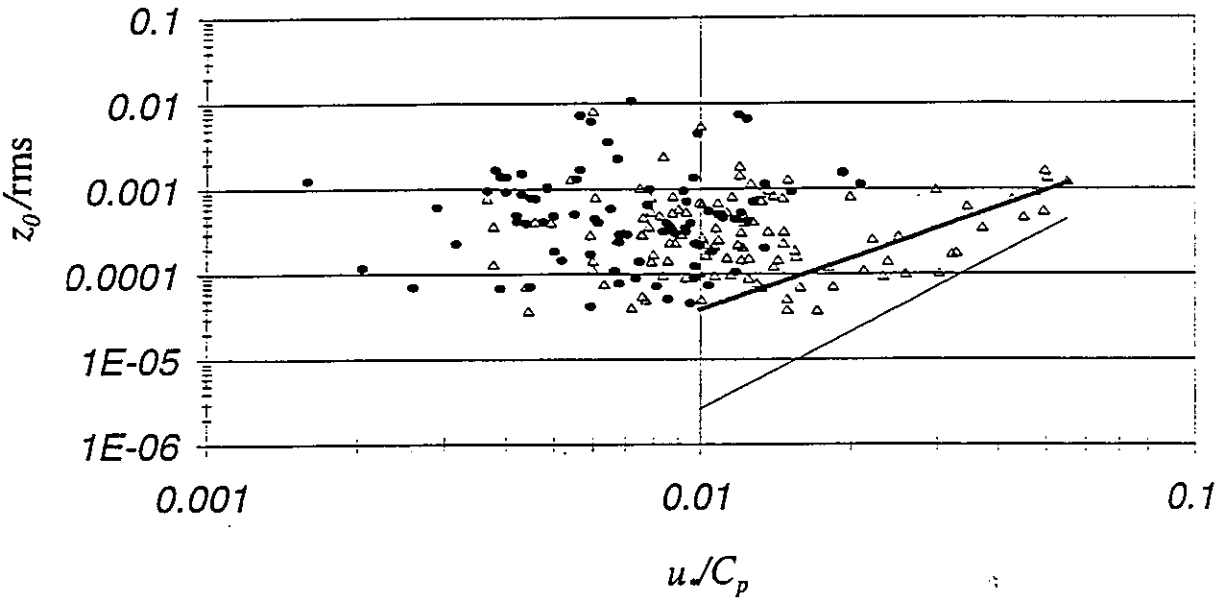


FIGURE 13. Dependence of normalized roughness (4 $z_0/H_{1/3}$) on inverse wave age. The two lines correspond to theoretical relations from Huang et al. (1986). The open triangles are for wind directions within 20° of 300°; the solid circles are for other wind directions.

We must explain why conditions with the largest wave ages have relatively greater stress than those with small wave ages when conventional wisdom and most models claim that young, growing waves extract more momentum from the wind than "equilibrium" waves. The answer is contained in the nature of the stress vector when the wind vector and the wave direction are not the same. Rieder et al. (1994) showed that the stress vector tends to lie in a direction between the wind and wave vectors and that the lighter the winds, the closer the stress vector approaches the wave direction. Furthermore, the conventional wisdom that young waves cause more stress is then consistent with our observations because it is the portion of the wave spectrum along the wind direction that is relevant to wave age. When the wind changes direction, there is an abrupt increase in stress as new small-scale waves are generated in the new direction. In other words, the stress is larger for winds blowing perpendicular to old gravity waves than when the winds blow in the swell direction. This interpretation becomes even more confusing in light winds when the roughness is dominated by gustiness, which may represent intermittent winds from many different directions.

## 6. CONCLUSIONS

Direct measurements of turbulent air-sea fluxes, surface wave parameters, and the structure of the CBL obtained from R/P *FLIP* during SCOPE in September 1993 are used for an investigation of the sea surface roughness length $z_0$ and the Charnock coefficient $\alpha$. Such parameterizations of the sea surface roughness length are important for atmosphere-ocean models, as well as for interpretation of remote sensing data.

A new approach was been developed for computation of $z_0$ under convective conditions usually associated with light winds. Note that stratification of the marine atmospheric surface layer is predominantly unstable and winds over the oceans are often light, especially in the tropical and coastal zones. The importance of using asymptotically correct forms for the dimensionless stability functions was clearly demonstrated and several misconceptions from earlier work were explained. It was shown that for unstable stratification different situations can be sorted into three regimes, for which three formulas for $z_0$ are applied: (i) the near neutral regime, Eq. (33); (ii) local free convection, Eq. (34); (iii) true free convection, Eq. (35). We also examined the fundamental matching conditions for turbulent and viscous sublayers in convective conditions and concluded that true free convection is rare over the ocean and the commonly accepted approach of separating roughness and stability considerations is almost always valid. A method for dealing with true convection when it occurs was developed, and software for doing the computations was written.

Analysis of SCOPE data showed that the roughness Reynolds number decreases as mean wind velocity decreases until about 4 m $s^{-1}$ (Fig. 7). As wind speeds decrease further, $Re_r$ remains constant or increases slightly but does not exceed the limit for rough flow as previously suggested by Wu (1994).

A mean value of the Charnock coefficient was found to be 0.0125 compared to 0.011 obtained from the tropical western Pacific (Fairall et al., 1995a). However, analysis of the Charnock coefficient indicates that $\alpha$ does not remain constant but begins to increase in the low wind-speed regime. This increase is shown to be associated with large swell propagating into the area so that local wind-wave balance is only achieved in a few stronger wind events. Restricting the wind direction to within 20° of the dominant direction reduces the estimated values for $\alpha$ to about a factor of two in the light wind regime, but it still remains significantly greater than 0.011. For light winds, when the mean wind direction is the same as the swell, the mean streamwise covariance stress is, in fact, zero, but the ocean still exhibits roughness and generates turbulence because of gustiness. A strong cross-stream stress covariance results from cases where the wind vector is different from the wave field. Our conclusion is that wind-stress vector assessments require more wave information than the simple parameters we have dealt with so far.

## 7. ACKNOWLEDGMENTS

This document has been generated as part of the joint NOAA/DOD Advanced Sensor Application Program (ASAP).

## 8. REFERENCES

Bourassa, M. A., D. G. Vincent, and W. L. Wood, 1995. A flux parameterization including the effects of capillary waves and sea state. *J. Atmos. Sci.* (submitted).

Businger, J. A., 1973. A note on free convection. *Boundary-Layer Meteorol.* **4**:323–326.

Businger, J. A., J. C. Wyngaard, Y. Izumi, and E. F. Bradley, 1971. Flux-profile relationships in the atmospheric surface layer. *J. Atmos. Sci.* **28**:181–189.

Charnock, H., 1955: Wind stress on a water surface. *Quart. J. Roy. Meteor. Soc.* **1**:639–640.

Deardorff, J. W., 1970: Convective velocity and temperature scales for the unstable planetary boundary layer and for Rayleigh convection. *J. Atmos. Sci.* **27**(8):1211–1213.

Delage, Y., and C. Girard, 1992. Stability functions correct at the free convection limit and consistent for both the surface and Ekman layers. *Boundary-Layer Meteorol.* **58**:19–31.

Fairall, C. W., J. B. Edson, S. E. Larsen, and P. G. Mestayer, 1990. Inertial-dissipation air-sea flux measurements: A prototype system using real-time spectral computations. *J. Atmos. Oceanic Technol.* **7**:425–453.

Fairall, C. W., E. F. Bradley, D. P. Rogers, J. B. Edson, and G. S. Young, 1995a. Air-sea flux parameterization in TOGA COARE. *J. Geophys. Res.*, accepted.

Fairall, C. W., A. B. White, J. B. Edson, and J. E. Hare, 1995b. Integrated shipboard measurements of the marine boundary layer. *J. Atmos. Oceanic Technol.* (submitted).

Geernaert, G. L., 1990. Bulk parameterizations for the wind stress and heat fluxes. In *Surface Waves and Fluxes,* Vol. 1. G. L. Geernaert and W. J. Plant (Eds.). Kluwer Academic, 336 pp.

Godfrey, J. S., and A. C. M. Beljaars, 1991. On the turbulent fluxes of buoyancy, heat, and moisture at the air-sea interface at low wind speeds. *J. Geophys. Res.* **96**:22,043–22,048.

Grachev, A. A., 1990. Friction law in the free-convection limit. *Izvestiya, Acad. Sci., USSR, Atmos. Oceanic Phys.* **26**(11):837–846 (English edition).

Hsu, S. A., 1974. A dynamic roughness equation and its application to wind stress determination at the air-sea interface. *J. Phys. Oceanogr.* **4**:116–120.

Huang, N. E., L. F. Bliven, S. R. Long, and P. S. DeLeonibus, 1986. A study of the relationship among wind speed, sea state, and the drag coefficient for a developing wave field. *J. Geophys. Res.* **91**(C6):7733–7742.

Kader, B. A., and A. M. Yaglom, 1990. Mean fields and fluctuation moments in unstably stratified turbulent boundary layers. *J. Fluid Mech.* **212**:637–662.

Kraichnan, R. H., 1962. Turbulent thermal convection at arbitrary Prandtl number. *Phys. Fluids*, **5**(11):1374–1389.

Kraus, E. B., and J. A. Businger, 1994. *Atmosphere-Ocean Interaction* (2nd edition). Oxford University Press, New York; Clarendon Press, Oxford, 362 pp.

Kropfli, R. A., and S. F. Clifford, 1994. The San Clemente Ocean Probing Experiment: A study of air-sea interactions with remote and in situ sensors. *Proc. IGARSS'94,* **IV**:2470–2409.

Liu, W. T., K. B. Katsaros, and J. A. Businger, 1979. Bulk parameterization of the air-sea exchange of heat and water vapor including the molecular constraints at the interface. *J. Atmos. Sci.* **36**:1722–1735.

Makin, V. K., V. N. Kudryavtsev, and C. Mastenbroek, 1995. Drag of the sea surface. *Boundary-Layer Meteorol.* **73**:159–182.

Monin, A. S., and A. M. Yaglom, 1971. *Statistical Fluid Mechanics: Mechanics of Turbulence*, Vol. 1. MIT Press, Cambridge, Massachusetts, 769 pp.

Panofsky, H. A., 1963. Determination of stress from wind and temperature measurements. *Quart. J. Roy. Meteor. Soc.* **89**:85–94.

Paulson, C. A., 1970. The mathematical representation of wind speed and temperature profiles in the unstable atmospheric surface layer. *J. Appl. Meteorol.* **9**:857–861.

Pierson, W. J., 1990. Dependence of radar backscatter on environmental parameters. In *Surface Waves and Fluxes*, Vol. II. G. L. Geernaert and W. J. Plant (Eds.). Kluwer Academic, 173–220.

Rieder, K. F., J. K. Smith, and R. A. Weller, 1994. Observed directional characteristics of the wind, wind stress, and surface waves on the open ocean. *J. Geophys. Res.* **99**(C11): 22,589–22,596.

Schumann, U., 1988. Minimum friction velocity and heat transfer in the rough surface layer of a convective boundary layer. *Boundary-Layer Meteorol.* **44**:311–326.

Smith, S. D., 1988. Coefficients for sea surface wind stress, heat flux, and wind profiles as a function of wind speed and temperature. *J. Geophys. Res.* **93**:15,467–15,472.

Smith, S. D., R. J. Anderson, W. A. Oost, C. Kraan, N. Maat, J. DeCosmo, K. B. Katsaros, K. L. Davidson, K. Bumke, L. Hasse, and H. M. Chadwick, 1992. Sea surface wind stress and drag coefficients: The HEXOS results. *Boundary-Layer Meteorol.* **60**:109–142.

Stull, R. B., 1994. A convective transport theory for surface fluxes. *J. Atmos. Sci.* **51**(1):3–22.

Sugita, M., T. Hiyama, N. Endo, and Shao-Fen Tian, 1995. Flux determination over a smooth surface under strongly unstable conditions. *Boundary-Layer Meteorol.* **73**:145–158.

Sykes, R. I., D. S. Henn, and W. S. Lewellen, 1993. Surface-layer description under free-convection conditions. *Quart. J. Roy. Meteor. Soc.* **119**:409–421.

Toba, Y., and M. Koga, 1986. A parameter describing overall conditions of wave breaking, whitecapping, sea-spray production, and wind stress. In *Oceanic Whitecaps*. E. C. Monahan and G. Mac Niocaill (Eds.). D. Reidel Publishing Company, 37–47.

Volkov, Yu A., A. A. Grachev, and D. T. Matveev, 1992. Transition from aerodynamically smooth to rough flow over the sea surface. *Izvestiya, Russian Acad. Sci., Atmos. Oceanic Phys.* **28**(7):580–583 (English edition).

Wu, Jin, 1994. The sea surface is aerodynamically rough even under light winds. *Boundary-Layer Meteorol.* **69**:149–158.

Zilitinkevich, S. S., 1994. Heat and mass transfer in convective atmosphere with weak winds. *J. Fluid Mech.* (submitted).

## Figure Captions

FIGURE 1a. Matching of the velocity profiles for the turbulent layer [Eq. (11), dashed line] and the viscous sublayer [Eq. (28), solid line] based on the LKB model. M indicates the matching point; C, the transition to the convective part of the profile; and Z, the height of the measurement for $u(z_r) = 4$ m s$^{-1}$, $\Delta T = 2.5$ K, $Re = 0.35$, and $C_u = 12.2$.

FIGURE 1b. Matching of the velocity profiles for the turbulent layer [Eq. (11), dashed line] and the viscous sublayer [Eq. (28), solid line] based on the LKB model. M indicates the matching point; C, the transition to the convective part of the profile; and Z, the height of the measurement for $u(z_r) = 0.5$ m s$^{-1}$, $\Delta T = 2.5$ K, $Re = 0.113$, and $C_u = 15.5$.

FIGURE 1c. Matching of the velocity profiles for the turbulent layer [Eq. (11), dashed line] and the viscous sublayer [Eq. (28), solid line] based on the LKB model. M indicates the matching point; C, the transition to the convective part of the profile; and Z, the height of the measurement for $u(z_r) = 0.25$ m s$^{-1}$, $\Delta T = 4$ K, $Re = 0.113$, and $C_u = 15.3$.

FIGURE 2. Atmospheric surface-layer observations made from R/P *FLIP* for 12 days during SCOPE: friction velocity $u_*$ (lower panel), mean wind velocity $u$ (line) and direction (dots), evaporation duct height, air temperature (line), and sea surface temperature (dots, upper panel). Julian day 261 corresponds to September 18, 1993.

FIGURE 3. Time series of friction velocity $u_*$ (lower panel), the ratio $u/u_*$, and the Monin-Obukhov stability profile correction $\Psi_u(\xi)$ using (11) and (17). Julian day 261 corresponds to September 18, 1993.

FIGURE 4. Charnock constant, $\alpha$, versus bulk-derived roughness Reynolds number, $Re_r$, for the COARE data (Fairall et al., 1995a). The dashed line corresponds to a mean value of $\alpha = 0.011$.

FIGURE 5. Charnock constant, $\alpha$, versus mean wind speed for SCOPE data (mean value, $\alpha = 0.0125$).

FIGURE 6. Individual data points (50-min averages) of the sea surface roughness length, $z_0$, as a function of the 11-m wind speed for SCOPE data. The values of $z_0$ are estimated from (27) for $\xi \leq -0.08$ and from (3) for $\xi \geq -0.08$. The solid line links mean value points that have been averaged in wind-speed bins with 1 m s$^{-1}$ width.

FIGURE 7. Individual data points (50-min averages) of the roughness Reynolds number, $Re_r$, as a function of the 11-m wind speed for SCOPE data. The solid line links mean value points that have been averaged in wind-speed bins with 1 m s$^{-1}$ width.

FIGURE 8. Individual data points (50-min averages) of the Charnock constant, $\alpha$, as a function of the 11-m wind speed for SCOPE data. The solid line links mean value points that have been averaged in wind-speed bins with 1 m $s^{-1}$ width.

FIGURE 9. The time series of the friction velocity, $u_*$ (thin line), wave phase speed, $C_p$ (heavy line), and significant wave height, $H_{1/3}$ (triangles), obtained during SCOPE.

FIGURE 10. Significant wave height $H_{1/3}$ versus the mean wind speed at 11 m. The lines are empirical dependences taken from Pierson (1990).

FIGURE 11. Charnock coefficient as a function of wind direction.

FIGURE 12. Dependence of $\alpha$ on wave age, $C_p/u_*$. The solid line is a regression of the form $\alpha = 0.48\ (C_p/u_*)^1$ from Smith et al. (1992). The open triangles are for wind directions within 20° of 300°; the solid circles are for other wind directions.

FIGURE 13. Dependence of normalized roughness ($4\ z_0/H_{1/3}$) on inverse wave age. The two lines correspond to theoretical relations from Huang et al. (1986). The open triangles are for wind directions within 20° of 300°; the solid circles are for other wind directions.



• U.S. GOVERNMENT PRINTING OFFICE 1996-0-774-018/40012